

# Multivoxel Proton MR Spectroscopy Used to Distinguish Anterior Cingulate Metabolic Abnormalities in Patients with Schizophrenia<sup>1</sup>

Caitlin J. Hardy, MD  
Assaf Tal, PhD  
James S. Babb, PhD  
Nissa N. Perry, MA  
Julie W. Messinger, MA  
Daniel Antonius, PhD  
Dolores Malaspina, MD  
Oded Gonen, PhD

## Purpose:

To test the hypothesis that anterior cingulate cortex (ACC) subregions in patients with schizophrenia are metabolically different from those in healthy control subjects.

## Materials and Methods:

This institutional review board–approved study was HIPAA compliant, and all participants provided written informed consent. Twenty-two patients with schizophrenia (13 male, nine female; 39.4 years  $\pm$  10.6 [standard deviation]) and 11 age- and sex-matched control subjects (seven male, four female; 35.5 years  $\pm$  10.7) underwent magnetic resonance (MR) imaging and three-dimensional 3-T voxel proton MR spectroscopy to measure absolute rostral and caudal ACC *N*-acetylaspartate (NAA), creatine (Cr), and choline (Cho) concentrations. Exact Mann-Whitney test was used to compare patient data with control data, paired-sample Wilcoxon signed rank test was used to compare subregions within groups, and receiver operating characteristic curve analysis was used to assess sensitivity and specificity in diagnosis of schizophrenia.

## Results:

There were no significant metabolic differences between patients and control subjects or between ACC subregions in control subjects. In patients, rostral ACC NAA and Cr concentrations were significantly lower than those in caudal ACC (6.2 mM  $\pm$  1.3 vs 7.1 mM  $\pm$  1.3,  $P < .01$ ; 5.7 mmol/L  $\pm$  1.4 vs 6.3 mmol/L  $\pm$  1.6,  $P < .01$ ; respectively); however, this did not hold true for Cho concentrations (1.7 mmol/L  $\pm$  0.5 vs 1.8 mmol/L  $\pm$  0.5). For individual differences between caudal and rostral measurements, only NAA in patients was different from that in control subjects (0.9 mmol/L  $\pm$  1.3 vs  $-0.1$  mmol/L  $\pm$  0.5,  $P < .01$ ), enabling prediction of schizophrenia with 68% sensitivity and 91% specificity, for a difference of more than 0.4.

## Conclusion:

Significant differences between caudal and rostral NAA concentration are found in ACC of patients with schizophrenia but not in ACC of healthy control subjects, indicating that neuronal density or integrity differences between ACC subregions may be characteristic of the disease.

© RSNA, 2011

<sup>1</sup>From the Departments of Radiology (C.J.H., A.T., J.S.B., N.N.P., O.G.) and Psychiatry (C.J.H., J.W.M., D.A., D.M.), New York University School of Medicine, 660 First Ave, 4th Floor, New York, NY, 10016; and Institute for Social and Psychiatric Initiatives, New York, NY (J.W.M., D.A., D.M.). Received March 31, 2011; revision requested May 11; revision received May 27; accepted June 7; final version accepted June 20. Address correspondence to O.G. (e-mail: [oded.gonen@med.nyu.edu](mailto:oded.gonen@med.nyu.edu)).

**S**chizophrenia, which is a chronic debilitating psychiatric disorder with an early age of onset, affects an estimated 1% of the population (1). Its direct treatment-related costs and indirect, mostly unemployment-related costs are estimated at \$23 billion and \$32 billion, respectively, in the United States alone (2). Although psychotic symptoms are well recognized in patients with schizophrenia, the prognosis is related to the negative symptoms of schizophrenia, which include a diminished motivation to initiate or persist in goal-directed behaviors and lower emotional expression. These features were first described as the core of the disorder by Kraepelin in 1919 (3), but their neural underpinnings remain uncertain and refractory to existing treatments (4,5). To facilitate new treatments for schizophrenia, it is imperative to advance our understanding of its biology and develop radiologic markers with which to monitor it.

Schizophrenia is associated with abnormalities of the anterior cingulate

cortex (ACC), which is a limbic structure with two functionally distinct subregions (6,7). It is an intriguing region with respect to volition and emotional expression. The rostral emotion-oriented portion lies just anterior to the genu of the corpus callosum, while the caudal cognition-oriented area is found just superior to the body of the corpus callosum, as shown in Figure 1 (7). Volumetric studies have shown that both of these anatomic subregions are smaller in patients with schizophrenia than in control subjects (6,8), with the degree of volume loss correlated to the severity of negative symptoms in the rostral ACC (9) and to positive symptoms in the caudal ACC (10). Functional MR imaging, in which subjects engaged in emotional and cognitive tasks, revealed abnormal activity in both ACC segments in patients with schizophrenia (11–13).

<sup>1</sup>H MR spectroscopy has also been used to study the ACC in patients with schizophrenia (14). The most common metabolites studied have been *N*-acetylaspartate (NAA), which is found only in neurons and is therefore considered a marker of their integrity (15,16); creatine (Cr) and phosphocreatine, which participate in adenosine triphosphate synthesis and represent the energy reserves of the cells (15,16); and choline (Cho) and phosphocholine, which are markers of membrane turnover (15,16).

Previous <sup>1</sup>H MR spectroscopic studies of NAA in the ACC of patients with schizophrenia have yielded inconsistent results. Some have revealed decreased NAA concentrations (14,17,18), while others have demonstrated positive correlation with executive function and negative correlation with positive symptoms, such as delusions, disorganization, and persecution (19,20).

#### Implication for Patient Care

- These findings may yield patient-specific information for use in the development of individualized approaches with which to treat schizophrenia that could lead to the identification of additional therapeutic targets for this disease.

In the current study, we compared absolute NAA, Cr, and Cho concentrations within their rostral and caudal ACC subregions by using three-dimensional (3D) multivoxel <sup>1</sup>H MR spectroscopy. This enabled us to obtain spectra from both ACC subregions in one examination, to more accurately include the structure despite its irregular shape, and to provide increased signal-to-noise ratio and, therefore, quantification accuracy when compared with single-voxel spectroscopy (21). Our objective was to test the hypothesis that ACC subregions in patients with schizophrenia are metabolically different from those in healthy control subjects.

#### Materials and Methods

##### Human Subjects

In this prospective study, 29 patients (18 male, 11 female; mean age, 40.6 years ± 10.7) with a diagnosis of schizophrenia were serially recruited from the outpatient clinic of New York University Hospital and Bellevue Hospital

#### Advances in Knowledge

- Three-dimensional multivoxel proton spectroscopy yields metabolite concentrations in the entire anterior cingulate cortex (ACC), including the irregularly shaped caudal and rostral subregions.
- Mean *N*-acetylaspartate (NAA) and creatine concentrations are significantly lower in the rostral ACC than in the caudal ACC in patients with schizophrenia, but they are not significantly lower in control subjects; these discrepancies in metabolite concentrations are consistent with the decreased energy requirement and the number and/or function of neurons in the rostral ACC compared with the caudal ACC.
- The difference in NAA concentration between the caudal ACC and the rostral ACC in individual subjects is significantly greater in patients with schizophrenia than in healthy subjects.

#### Published online before print

10.1148/radiol.11110675 Content code: **NR**

Radiology 2011; 261:542–550

#### Abbreviations:

ACC = anterior cingulate cortex

Cho = choline

Cr = creatine

CSF = cerebrospinal fluid

NAA = *N*-acetylaspartate

3D = three dimensional

VOI = volume of interest

#### Author contributions:

Guarantors of integrity of entire study, D.M., O.G.; study concepts/study design or data acquisition or data analysis/interpretation, all authors; manuscript drafting or manuscript revision for important intellectual content, all authors; manuscript final version approval, all authors; literature research, C.J.H., D.A., D.M., O.G.; clinical studies, C.J.H., N.N.P., D.M.; experimental studies, C.J.H., D.M., O.G.; statistical analysis, C.J.H., A.T., J.S.B.; and manuscript editing, C.J.H., A.T., J.S.B., J.W.M., D.A., D.M., O.G.

#### Funding:

This research was supported by the National Institutes of Health (grants NS050520, EB01015, RC1MH088843, and MH01699).

Potential conflicts of interest are listed at the end of this article.

Figure 1

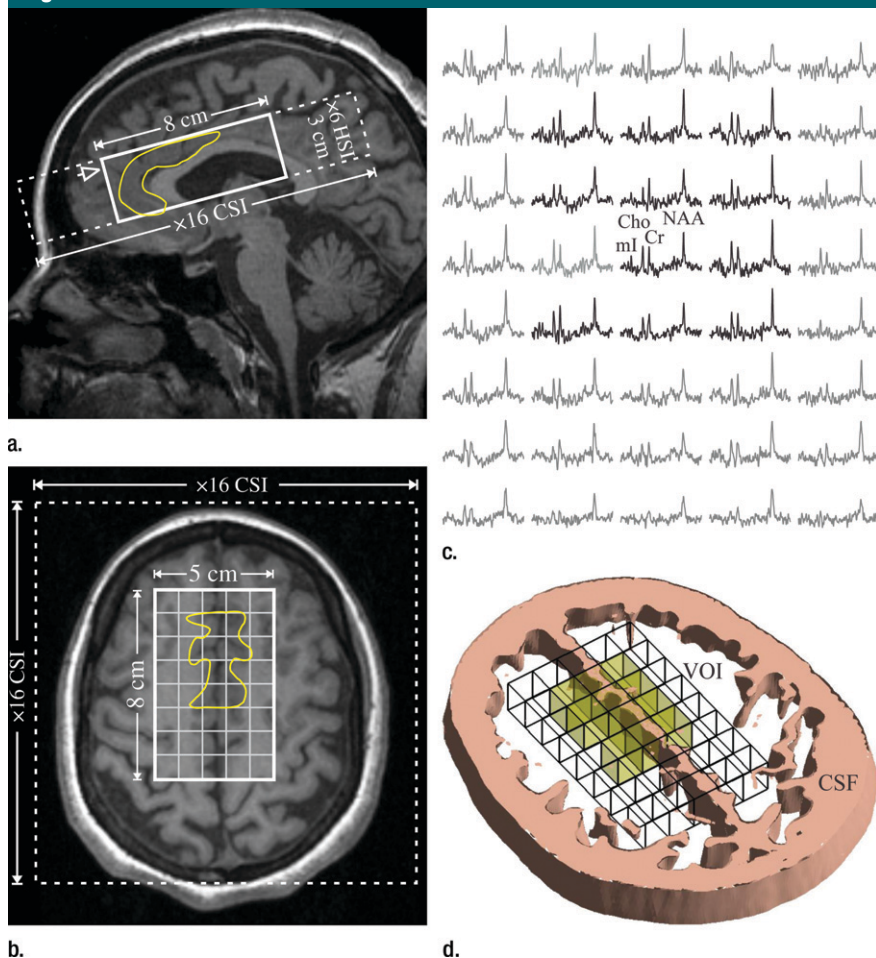


**Figure 1:** (a) Sagittal and (b) axial T1-weighted magnetic resonance (MR) images in a 30-year-old woman with schizophrenia (patient 18 in Table 1) superimposed with the  $5 \times 8 \times 3$ -cm (left-right direction  $\times$  anterior-posterior direction  $\times$  inferior-superior direction) volume of interest (VOI) (solid line),  $16 \times 16$ -cm (left-right direction  $\times$  anterior-posterior direction) axial chemical shift imaging (CSI) field of view (dashed line), and anterior cingulate gyrus (yellow line). Open arrow in **a** denotes level of **b**. (c) Real part of the five-voxel by eight-voxel axial proton ( $^1\text{H}$ ) spectra matrix from VOI in **b**. Spectra represent  $0.5\text{-cm}^3$  voxels, and all are on common frequency and intensity scales. Spectra within the anterior cingulate gyrus are black, while remaining spectra (not included in analysis) are gray. None of the ACC involves VOI edge voxels that have chemical shift displacement and the good signal-to-noise ratio and excellent spectral resolution (line width,  $5.3 \text{ Hz} \pm 1.2$  [standard deviation]) from these high-spatial-resolution voxels. (d) Cerebrospinal fluid (CSF) mask generated with statistical parametric mapping software from the five magnetization-prepared rapid gradient-echo sections that overlap the  $0.5\text{-cm-thick}$   $^1\text{H}$  MR spectroscopic section in **c**, superimposed with the VOI chemical shift imaging grid. CSF fraction was estimated for each voxel by adding all its fractions in the 500 mask pixels within it. Voxels chosen for analysis are yellow and correspond to those selected in **c**.

(New York, NY) between February 2010 and January 2011. Eleven age- and sex-matched healthy control subjects (seven male, four female; mean age,  $35.5 \text{ years} \pm 10.7$ ) were recruited via medical center postings. Inclusion criteria for patients were age between 18 and 60 years,

diagnosis of schizophrenia (or schizoaffective disorder), and capacity to provide informed consent. Exclusion criteria were uncontrolled medical illness, presence of a neurologic condition, substance abuse in the past 6 months, and any contraindication to MR imaging.

Additional exclusion criteria for control subjects were history of axis I disorders or family history of psychosis. A total of seven patients were excluded; three were excluded because of excessive uncontrollable motion (probably related to medication) during the examination, and four were excluded because of poor spectra quality. This left us with 22 patients (13 male, nine female; mean age,  $39.4 \text{ years} \pm 10.6$ ) for analysis. No control subjects were excluded. Characteristics of all patients and control subjects are shown in Table 1.

All patients and control subjects were assessed with the Diagnostic Interview for Genetic Studies, which was administered by interviewers with a master's degree or higher (J.W.M., D.A., D.M.; 3, 5, and 20 years of experience, respectively) who had been trained to meet standards of reliability (22). This institutional review board-approved study was compliant with the Health Insurance Portability and Accountability Act, and all participants provided written informed consent.

### MR Data Acquisition

All experiments were performed with a 3-T whole-body MR imager (Trio; Siemens, Erlangen Germany) and a transmit-receive head coil (TEM3000; MR Instruments, Minneapolis, Minn). For anatomic reference and guidance of the spectroscopic VOI, we obtained 3D T1-weighted magnetization-prepared rapid gradient-echo MR images with the following parameters: repetition time msec/echo time msec/inversion time msec,  $1360/2.6/800$ ; matrix,  $256 \times 256$ ; and field of view,  $256 \times 256 \text{ mm}$ . We acquired 160  $1\text{-mm-thick}$  sections in each participant. The images were reformatted into 192 sections, each  $1 \text{ mm}$  thick, in axial, sagittal, and coronal orientations to yield isotropic  $1\text{-mm}^3$  pixels.

We used the chemical shift imaging-based automatic procedure to adjust the first- and second-order shims in 3–5 minutes (23). A  $120\text{-cm}^3$  ( $8 \text{ cm}$  anterior-posterior direction  $\times 5 \text{ cm}$  left-right direction  $\times 3 \text{ cm}$  inferior-superior direction) parallelepiped  $^1\text{H}$  MR spectroscopic VOI was then guided with imaging over the ACC, as shown in

Figure 1. This VOI was excited by using point-resolved spectroscopy (repetition time msec/echo time msec, 1800/35) with three second-order Hadamard-encoded slabs (six sections) interleaved along the inferior-superior direction for every repetition time for optimal signal-to-noise ratio and spatial coverage (24). Interleaving also enabled us to apply a strong 9 mT/m Hadamard section-select gradient to reduce the chemical shift displacement between NAA and Cho to approximately 0.13 mm (approximately 3% of the section thickness) (25). Such thin sections were chosen to reduce the line-broadening effects of the strong, 1–2 ppm/cm static magnetic field susceptibility gradients in the inferior-superior direction from the air-tissue interface with the nearby maxillary sinuses just underneath, as seen in Figure 1a (26,27).

The Hadamard-defined planes of the six sections were encoded with  $16 \times 16$  two-dimensional chemical shift imaging over a  $16 \times 16$ -cm (left-right direction  $\times$  anterior-posterior direction) field of view to form  $1.0 \times 1.0 \times 0.5$ -cm voxels. The VOI in these planes was defined by two 11.2-msec-long numerically optimized  $180^\circ$  pulses of less than 1.35 mT/m in the anterior-posterior direction and less than 2.16 mT/m in the left-right direction to yield 240 voxels (five left-right voxels  $\times$  eight anterior-posterior voxels  $\times$  six inferior-superior voxels), as shown in Figure 1c. Although these gradients lead to a chemical shift displacement between NAA and Cho of 2.6 mm in the anterior-posterior direction and 1.5 mm in the left-right direction (26% and 15% voxel size, respectively), these occur only at VOI edges. For this reason, we increased the VOI beyond the ACC size (Fig 1b) to relegate this error to only those voxels that were to be excluded from analyses anyway. Also note that although the actual voxel size (full width at half maximum of the point spread function) for this uniform two-dimensional phase encoding was  $0.63 \text{ cm}^3$  ( $1.12 \text{ cm} \times 1.12 \text{ cm} \times 0.5 \text{ cm}$ ) (28,29), since the nominal voxel size is equal to the actual voxel size in the Hadamard direction (30), we will continue to refer to the nominal size for

Table 1

## Characteristics for All Subjects and Patients

Participant No. and Group	Age (y)	Sex	Disease Duration (mo)	Psychotropic Medication
<b>Control</b>				
1	21	F	NA	NA
2	23	M	NA	NA
3	28	M	NA	NA
4	29	F	NA	NA
5	31	M	NA	NA
6	33	F	NA	NA
7	36	M	NA	NA
8	43	M	NA	NA
9	45	M	NA	NA
10	47	M	NA	NA
11	55	F	NA	NA
<b>Patient</b>				
12	22	M	48	Clozapine
13	23	M	36	Risperidone
14	25	M	60	Clozapine, valproic acid
15	26	M	96	Ziprasidone
16	28	M	108	Clomipramine, risperidone, clonazepam
17	29	F	96	Bupropion, aripiprazole, fluphenazine
18	30	F	120	Risperidone
19	34	M	60	Risperidone
20	38	F	276	Clonazepam, fluphenazine
21	41	M	264	Fluphenazine
22	42	F	276	Ziprasidone, bupropion, eszopiclone
23	43	M	216	Halperidol, quetiapine
24	43	F	240	Aripiprazole, escitalopram, fluphenazine
25	44	M	312	Clozapine, valproic Acid
26	44	F	324	Quetiapine
27	44	M	384	Fluphenazine, ziprasidone
28	48	M	276	Quetiapine
29	51	F	180	NA
30	51	F	420	Gabapentin, lithium, ziprasidone
31	52	M	384	Citalopram
32	53	M	372	Venlafaxine, gabapentin, clozapine
33	55	F	432	Aripiprazole, trazadone, quetiapine

Note.— F = female, M = male, NA = not applicable.

consistency. The MR signal was acquired for 256 msec at  $\pm 1$  kHz bandwidth. At two averages, the  $^1\text{H}$  MR spectroscopic portion of the examination took 30 minutes, and the entire protocol lasted slightly less than 1 hour.

## MR Spectroscopic Postprocessing

A spectroscopist (O.G.) with 20 years of experience used in-house software to process MR spectroscopic data offline. Residual water was removed from the MR signals in the time domain (31),

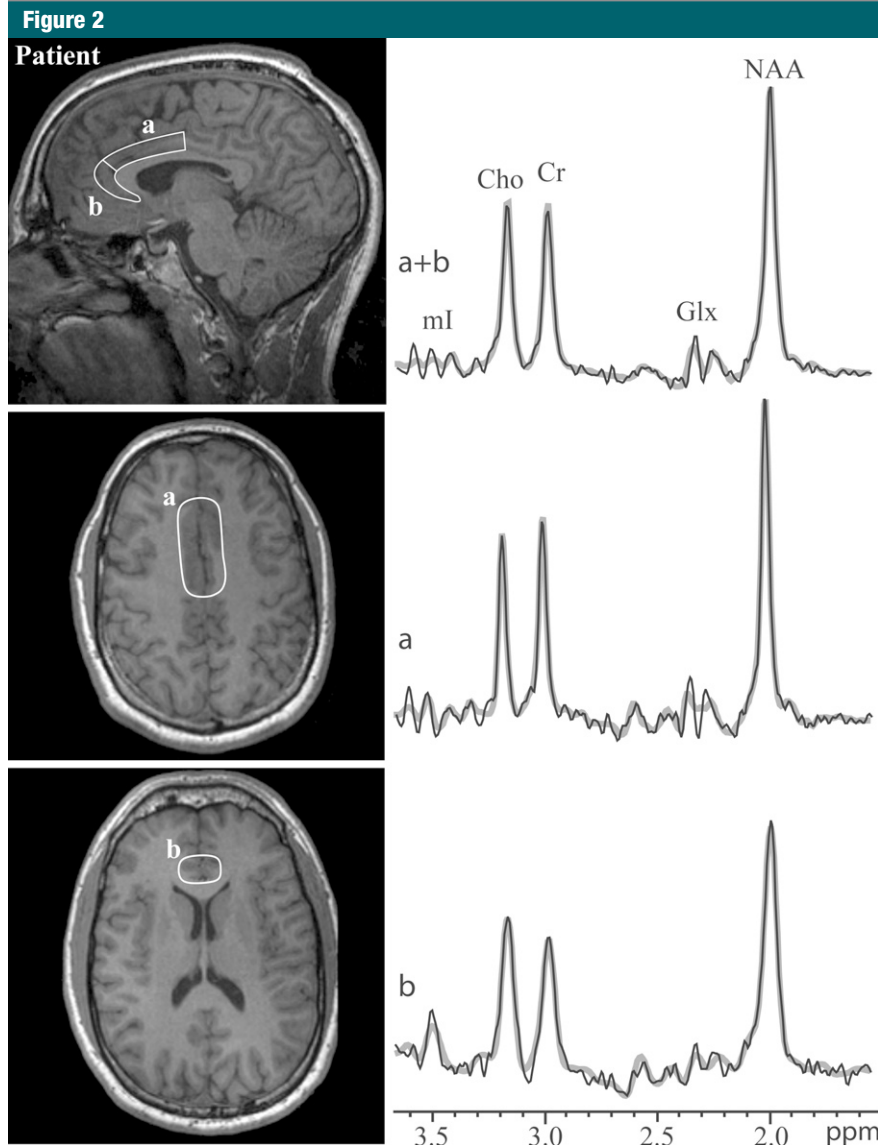


**Figure 2:** Left: Sagittal (top) and axial T1-weighted MR images at the caudal (center) and rostral (bottom) ACC level in a 26-year-old man with schizophrenia (patient 15 in Table 1). Caudal (a) and rostral (b) ACC are outlined. Irregular shape of the ACC makes 3D <sup>1</sup>H MR spectroscopy the appropriate probe. Right: Real part of <sup>1</sup>H spectra sums from all voxels within outlined regions of ACC on corresponding images (black line) superimposed with spectral fit function (gray line) with *myo*-inositol and glutamine and glutamate. All spectra are on the same frequency and intensity scales. Note the excellent signal-to-noise ratio of the spectra and the consequent good fit.

and the spectrum of each voxel was shifted to align the chemical shift imaging grid with the NAA VOI. The data were then Fourier transformed in the temporal, anterior-posterior, and left-right spatial directions, and Hadamard reconstruction was performed along the inferior-superior direction. Spectra were

automatically corrected for frequency and zero-order phase shifts in reference to the NAA peak in each voxel (32).

Because the VOI also contains CSF (Figs 1–3) in which the metabolite concentrations are lower than the detection threshold of <sup>1</sup>H MR spectroscopy, we used statistical parametric mapping

software (SPM8; Wellcome Department of Cognitive Neurology, Institute of Neurology, Queen Square, London, England) (33,34) to produce CSF masks from the axial magnetization-prepared rapid gradient-echo MR images. Subsequently, to correct for the CSF partial volume, we used in-house software (Matlab 2009b; Mathworks, Natick, Mass) to estimate the CSF fraction (CSF volume divided by voxel volume) in each of the 240 voxels in the VOI, as shown in Figure 1d. We estimated CSF fraction for each voxel by adding all CSF fractions in the 500 magnetization-prepared rapid acquisition gradient echo segmented mask pixels within it.

The caudal and rostral regions of the ACC were manually traced on the axial MR images of each subject, as shown in Figures 1–3. Our software then added the phased and aligned CSF normalized spectra from all the voxels that fell completely or partially within the circumscribed region, as shown in Figures 2 and 3. The relative concentrations of the *i*th (*i* = NAA, Cr, Cho) metabolite in the *j*th (*j* = 1.0.27) subject and *k*th (*k* = caudal or rostral) region were estimated from their peak area,  $S_{ijk}$ , by using the SITools-FIT parametric spectral modeling and least-squares optimization software described by Soher et al (35), as shown in Figures 2–4. Specifically, aspartate, glutamate, glutamine, Cho, Cr, *myo*-inositol, NAA, and taurine model functions were used to fit our data. The  $S_{ijk}$  was then scaled into absolute concentration,  $C_{ijk}$ , with phantom replacement relative to a 2-L sphere of in vitro concentration ( $C_{vit}^i$ )  $C_{i vit}^i = 12.5, 10.0, 3.0,$  and  $7.5$  mmol/L for NAA, Cr, Cho and *myo*-inositol, respectively in water at physiologic ionic strength:

$$C_{ijk} = C_{vit}^i \cdot \frac{S_{ij}}{S_R} \cdot \frac{V_j^{180^\circ}}{V_R^{180^\circ}}, \quad [1]$$

where  $S_R$  is the signal of the phantom metabolites and  $V_j^{180^\circ}$  and  $V_R^{180^\circ}$  represent the radiofrequency voltage needed for a nonselective 1-msec 180° pulse on subject and reference, respectively.  $C_{ijk}$  was corrected for in vivo ( $T_1^{viv}, T_2^{viv}$ ) and

in vitro ( $T_1^{\text{vit}}$ ,  $T_2^{\text{vit}}$ ) T1 and T2 relaxation time differences with a factor (36):

$$f = \frac{\exp(-TE/T_2^{\text{vit}})}{\exp(-TE/T_2^{\text{vit}})} \cdot \frac{1 - \exp(-TR/T_1^{\text{vit}})}{1 - \exp(-TR/T_1^{\text{vit}})} \quad [2]$$

by using  $T_1^{\text{vit}}$  of 1.4, 1.3, and 1.2 msec;  $T_2^{\text{vit}}$  of 343, 172, and 248 msec;  $T_1^{\text{vit}}$  of 605, 336, and 235 msec; and  $T_2^{\text{vit}}$  of 483, 288, and 200 msec in the phantom. TE is echo time and TR is relaxation time. All measurements correspond to NAA, Cr, and Cho at 3 T, respectively (37–39).

### Statistical Analyses

An exact Mann-Whitney test was used to compare groups with respect to the mean concentration of each metabolite within each region. A paired-sample Wilcoxon signed rank test was used to compare dorsal and rostral regions in terms of the metabolite concentrations within each group. Receiver operating characteristic curve analysis was used to assess the diagnostic utility of the measures in the discrimination of patients from control subjects. Reported values of sensitivity and specificity are from the cutoff value observed to maximize the average of these components of diagnostic accuracy. All reported  $P$  values are two-sided and indicate a significant difference if  $P \leq .05$ . We used statistical software (SAS, version 9.3; SAS Institute, Cary NC) for all computations.

### Results

Our shimming procedure yielded metabolites with a voxel line width of  $5.3 \text{ Hz} \pm 1.2$  for all patients and control subjects, as shown in Figure 1. Examples of the manually traced ACC and its subregions and the spectra sums from all voxels that fell within these regions in a patient and a control subject are shown in Figures 2 and 3. Metabolite concentrations in the rostral, caudal, and total ACC of each group are compiled in Table 2.

Analysis by group revealed no differences between patients and control subjects in terms of metabolite concentration in rostral, caudal or total ACC.

**Figure 3**

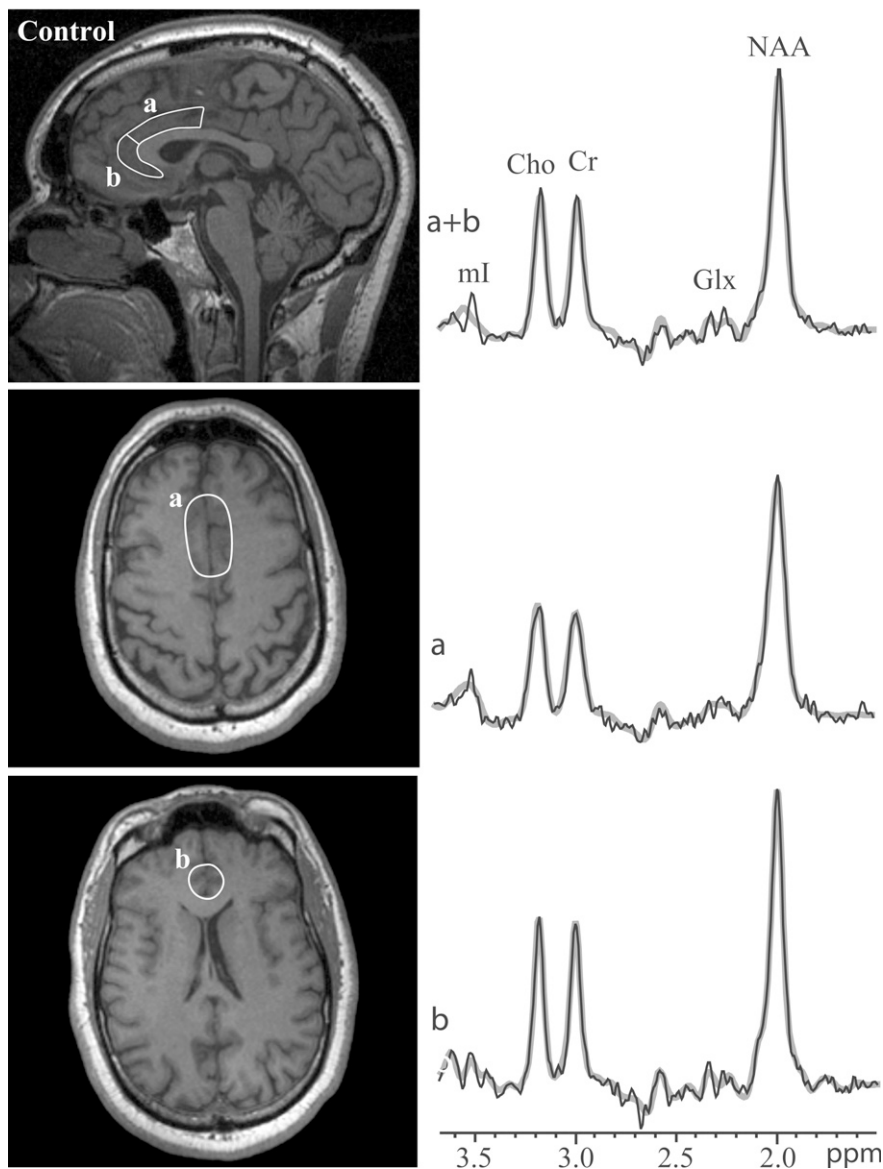


**Figure 3:** Left: Sagittal (top) and axial T1-weighted MR images at the caudal (center) and rostral (bottom) ACC level in a 47-year-old healthy man (control subject 10 in Table 1). Caudal (*a*) and rostral (*b*) ACC are outlined. Irregular shape of the ACC makes 3D  $^1\text{H}$  MR spectroscopy the appropriate probe. Right: Real part of  $^1\text{H}$  spectra sums from all voxels within outlined regions of ACC on corresponding images (black line) superimposed with spectral fit function (gray line) with *myo*-inositol and glutamine and glutamate. All spectra are on the same frequency and intensity scales. Note the excellent signal-to-noise ratio of the spectra and the quality of the fit.

Comparison of mean concentrations within each group, however, showed that patients had significantly lower mean NAA ( $P < .01$ ) and Cr ( $P < .01$ ) concentrations in the rostral ACC than in the caudal ACC (Table 2). No such differences were observed in control subjects.

Cho concentration did not vary between the two subregions in either group.

To investigate the relationship between the diagnosis and an individual subject's caudal–rostral differences, we defined a new metric,  $\Delta$ , which equals the difference between caudal and rostral

Figure 4

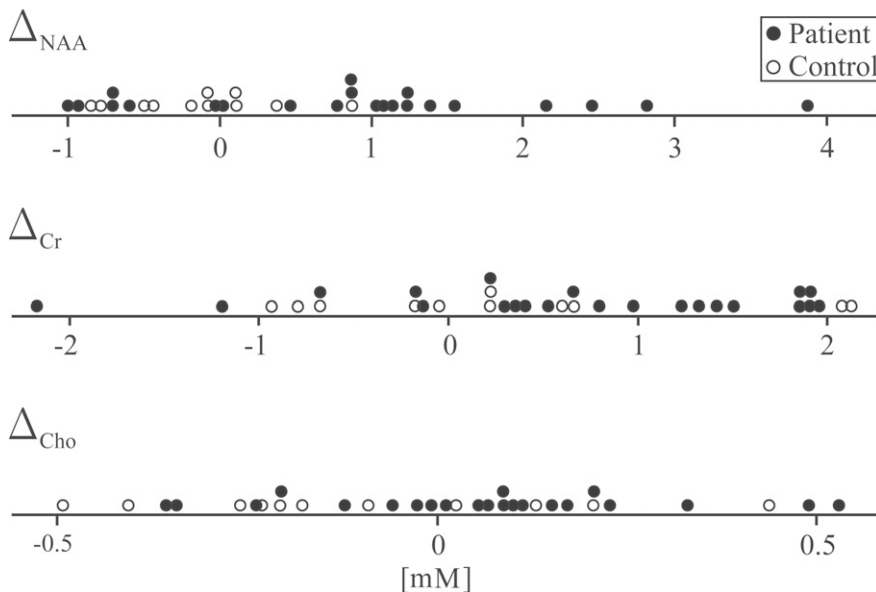


**Figure 4:** Dot plot of the distribution for individual caudal-rostral ACC concentration ( $\Delta$ ) in patients (●) and subjects (○) for NAA, Cr, and Cho concentrations. Note the significantly elevated  $\Delta_{\text{NAA}}$  in patients ( $0.9 \text{ mmol/L} \pm 1.3$  in patients vs  $-0.1 \text{ mmol/L} \pm 0.5$  in subjects,  $P < .01$ ). ROC analysis showed that  $\Delta_{\text{NAA}}$  greater than 0.4 could be used to predict schizophrenia with 68% sensitivity and 91% specificity.

concentrations. The distributions of caudal-rostral concentrations of NAA ( $\Delta_{\text{NAA}}$ ), Cr ( $\Delta_{\text{Cr}}$ ), and Cho ( $\Delta_{\text{Cho}}$ ) are shown in Figure 4. Only  $\Delta_{\text{NAA}}$  differed significantly between patients and control subjects ( $0.9 \text{ mmol/L} \pm 1.3$  vs  $-0.1 \text{ mmol/L} \pm 0.5$ ,  $P < .05$ ). Analysis of the ROC curve revealed only  $\Delta_{\text{NAA}}$  was a predictor of schizophrenia, with 68% sensitivity (15 of 22 patients had true-positive findings) and 91% specificity (10 of 11 control subjects had true-negative findings) for  $\Delta_{\text{NAA}}$  of more than 0.4 mmol/L, with an area under the curve of 0.74 (95% confidence interval: 0.57, 0.89). The area under the curve for both  $\Delta_{\text{Cr}}$  (0.62; 95% confidence interval: 0.45, 0.79) and  $\Delta_{\text{Cho}}$  (0.65; 95% confidence interval: 0.49, 0.82) was considered poor.

### Discussion

By probing the entire irregular shape of the ACC during one high-spatial-resolution 3D  $^1\text{H}$  MR spectroscopic examination, one may directly compare the rostral (emotional) and caudal (cognitive) regions within a patient. This comparison

reveals significant differences in NAA concentration between subregions in patients with schizophrenia that are not present in healthy control subjects. This finding most likely represents the relatively decreased cellular density in the rostral ACC when compared with that in the caudal ACC seen during postmortem studies that reveal decreased neuron density in the rostral ACC (6,40) but unchanged (6,41,42) or even increased (43) neuron density in the caudal region in patients with schizophrenia.

ACC subregional metabolic quantification may have important implications for development of drugs used to treat schizophrenia. Much of our current understanding of psychotropic medications has come from observing their effects on clinical symptoms. There is only a limited understanding of the underlying mechanism(s) of action and few, if any, clinically available methods with which to monitor activity in desired brain regions (44). The ability to localize biochemical changes, therefore, is desirable to understand the mechanism of established therapies and to monitor the response to novel

Table 2

### Absolute NAA, Cr, and Cho Concentrations in Caudal, Rostral, and Total Anterior Cingulate Gyrus

Metabolite and Region	Control Subjects (mmol/L)	Patients (mmol/L)
<b>NAA</b>		
Caudal	$6.5 \pm 1.1$	$7.1 \pm 1.63$
Rostral	$6.6 \pm 0.8$	$6.2 \pm 1.3$
Total	$6.6 \pm 0.9$	$6.5 \pm 1.2$
<b>Cr</b>		
Caudal	$5.8 \pm 1.1$	$6.3 \pm 1.6$
Rostral	$5.5 \pm 0.8$	$5.7 \pm 1.4$
Total	$5.6 \pm 0.8$	$5.9 \pm 1.3$
<b>Cho</b>		
Caudal	$1.6 \pm 0.3$	$1.8 \pm 0.5$
Rostral	$1.7 \pm 0.3$	$1.7 \pm 0.5$
Total	$1.6 \pm 0.3$	$1.7 \pm 0.4$

Note.—Data are means  $\pm$  standard deviations. There were no significant differences between groups.

ones. Since current antipsychotic medications have minimal efficacy in the treatment of the negative and cognitive symptoms of schizophrenia (45), and given that negative symptoms are linked to the rostral ACC and cognitive symptoms are linked to the caudal ACC, both areas separately are likely attractive targets for new therapies and novel noninvasive markers (9,13).

To our knowledge, in only one other study have researchers compared rostral and caudal metabolite concentrations in patients with schizophrenia by using two single voxels in each subregion (46). Wood et al (46) found significantly lower NAA concentrations in patients as compared with control subjects and in the rostral region as compared with the caudal region in both groups. Our finding of decreased NAA concentration in the rostral ACC of patients corroborates the findings of Wood et al (46). However, we did not reproduce others' findings of lower NAA (17,18,46,47) or Cr (48) concentrations in the ACC.

Disagreements with previous findings and the variable results of other  $^1\text{H}$  MR spectroscopic studies of the ACC in patients with schizophrenia may reflect methodologic differences between studies (20,49). Specifically, use of single voxels, whereby sensitivity

dictates volumes of 3.5 cm<sup>3</sup> or larger, is unable to effectively contain the irregular shape of the ACC; and must, consequently, suffer considerable subcortical white matter partial volume. The use of high-spatial-resolution 3D <sup>1</sup>H MR spectroscopy instead of single-voxel <sup>1</sup>H MR spectroscopy enabled us to better encompass the entire ACC and discern its caudal and rostral subregions in one examination while minimizing partial volume contamination from surrounding tissue.

Our study had several limitations. First, the relatively small sample did not enable us to account for the various phenotypes of schizophrenia, group patients into narrow age cohorts, or look for differences between male and female participants. Second, we did not control for the effects of medication. This limitation, however, is an unavoidable and nearly universal limitation in studies of patients with chronic schizophrenia. It represents a potential confounding factor, given the fact that there has been demonstration of decreased NAA concentration in the ACC of patients taking typical, but not atypical, antipsychotic medications (47). Third, although the voxels were relatively small, they were not sufficiently small to enable us to precisely trace the tortuous edges of the ACC, resulting in some partial volume of subcortical white matter at its surface. Although this is unavoidable, its effect is significantly less than that when larger single-voxels are used. Similarly, a small number of voxels at the rostral-caudal interface contained elements of both ACC subregions, leading to some unavoidable partial volume effects between them.

In conclusion, we probed the entire irregular shape of the ACC during one high-spatial-resolution 3D <sup>1</sup>H MR spectroscopic examination; this enabled us to compare the rostral and caudal regions within a subject and revealed significant differences in NAA concentrations in patients with schizophrenia that are not seen in healthy subjects. In consideration of the paucity of non-clinical (laboratory or radiologic) surrogate markers of schizophrenia, the distinctive pattern of metabolite variance

found between ACC regions in patients but not healthy control subjects may offer the potential to improve diagnostic accuracy and monitor therapeutic targets in this disease that affects approximately 1% of the population. In turn, these markers could provide us with guidance in developing and monitoring individualized treatment paradigms for schizophrenia.

**Acknowledgments:** We thank Andrew A. Maudsley of the University of Miami, Fla, and Brian J. Soher of Duke University, Durham, NC, for use of spectral modeling software. Assaf Tal acknowledges the support of the Human Frontiers Science Project.

**Disclosures of Potential Conflicts of Interest:** **G.J.H.** No potential conflicts of interest to disclose. **A.T.** Financial activities related to the present article: received a postdoctoral training fellowship from the Human Frontiers Science Project. Financial activities not related to the present article: none to disclose. Other relationships: none to disclose. **J.S.B.** No potential conflicts of interest to disclose. **N.N.P.** potential conflicts of interest to disclose. **J.W.M.** No potential conflicts of interest to disclose. **D.A.** No potential conflicts of interest to disclose. **D.M.** No potential conflicts of interest to disclose. **O.G.** No potential conflicts of interest to disclose.

## References

- Mueser KT, Penn DL. Meta-analysis examining the effects of social skills training on schizophrenia. *Psychol Med* 2004;34(7):1365-1367.
- Wu EQ, Birbaum HG, Shi L, et al. The economic burden of schizophrenia in the United States in 2002. *J Clin Psychiatry* 2005;66(9):1122-1129.
- Kraepelin E. *Dementia praecox and paraphrenia*. Huntington, NY: Krieger, 1971.
- Tamminga CA, Buchanan RW, Gold JM. The role of negative symptoms and cognitive dysfunction in schizophrenia outcome. *Int Clin Psychopharmacol* 1998;13(Suppl 3):S21-S26.
- Messinger JW, Trémeau F, Antonius D, et al. Avolition and expressive deficits capture negative symptom phenomenology: implications for DSM-5 and schizophrenia research. *Clin Psychol Rev* 2011;31(1):161-168.
- Fornito A, Yücel M, Dean B, Wood SJ, Pantelis C. Anatomical abnormalities of the anterior cingulate cortex in schizophrenia: bridging the gap between neuroimaging and neuropathology. *Schizophr Bull* 2009;35(5):973-993.
- Bush G, Luu P, Posner MI. Cognitive and emotional influences in anterior cingulate cortex. *Trends Cogn Sci* 2000;4(6):215-222.
- Baiano M, David A, Versace A, Churchill R, Balestrieri M, Brambilla P. Anterior cingulate volumes in schizophrenia: a systematic review and a meta-analysis of MRI studies. *Schizophr Res* 2007;93(1-3):1-12.
- Preuss UW, Zetsche T, Pogarell O, et al. Anterior cingulum volumetry, auditory P300 in schizophrenia with negative symptoms. *Psychiatry Res* 2010;183(2):133-139.
- Choi JS, Kang DH, Kim JJ, et al. Decreased caudal anterior cingulate gyrus volume and positive symptoms in schizophrenia. *Psychiatry Res* 2005;139(3):239-247.
- Taylor SF, Chen AC, Tso IF, Liberzon I, Welsh RC. Social appraisal in chronic psychosis: role of medial frontal and occipital networks. *J Psychiatr Res* 2011;45(4):526-538.
- Habel U, Chechko N, Pauly K, et al. Neural correlates of emotion recognition in schizophrenia. *Schizophr Res* 2010;122(1-3):113-123.
- Wilmsmeier A, Ohrmann P, Suslow T, et al. Neural correlates of set-shifting: decomposing executive functions in schizophrenia. *J Psychiatry Neurosci* 2010;35(5):321-329.
- Abbott C, Bustillo J. What have we learned from proton magnetic resonance spectroscopy about schizophrenia? a critical update. *Curr Opin Psychiatry* 2006;19(2):135-139.
- Gujar SK, Maheshwari S, Björkman-Burtscher I, Sundgren PC. Magnetic resonance spectroscopy. *J Neuroophthalmol* 2005;25(3):217-226.
- Ross B, Bluml S. Magnetic resonance spectroscopy of the human brain. *Anat Rec* 2001;265(2):54-84.
- Deicken RF, Zhou L, Schuff N, Weiner MW. Proton magnetic resonance spectroscopy of the anterior cingulate region in schizophrenia. *Schizophr Res* 1997;27(1):65-71.
- Bustillo JR, Rowland LM, Mullins P, et al. <sup>1</sup>H-MRS at 4 tesla in minimally treated early schizophrenia. *Mol Psychiatry* 2010;15(6):629-636.
- Premkumar P, Parbhakar VA, Fannon D, et al. N-acetyl aspartate concentration in the anterior cingulate cortex in patients with schizophrenia: a study of clinical and neuropsychological correlates and preliminary exploration of cognitive behaviour therapy effects. *Psychiatry Res* 2010;182(3):251-260.
- Ohrmann P, Kugel H, Bauer J, et al. Learning potential on the WCST in schizophrenia is related to the neuronal integrity of the

- anterior cingulate cortex as measured by proton magnetic resonance spectroscopy. *Schizophr Res* 2008;106(2-3):156-163.
21. Kreis R. Issues of spectral quality in clinical 1H-magnetic resonance spectroscopy and a gallery of artifacts. *NMR Biomed* 2004;17(6):361-381.
  22. Nurnberger JI Jr, Blehar MC, Kaufmann CA, et al. Diagnostic interview for genetic studies: rationale, unique features, and training—NIMH Genetics Initiative. *Arch Gen Psychiatry* 1994;51(11):849-859; discussion 863-864.
  23. Hu J, Javaid T, Arias-Mendoza F, Liu Z, McNamara R, Brown TR. A fast, reliable, automatic shimming procedure using 1H chemical-shift-imaging spectroscopy. *J Magn Reson B* 1995;108(3):213-219.
  24. Goelman G, Liu S, Hess D, Gonen O. Optimizing the efficiency of high-field multivoxel spectroscopic imaging by multiplexing in space and time. *Magn Reson Med* 2006;56(1):34-40.
  25. Goelman G, Liu S, Fleysher R, Fleysher L, Grossman RI, Gonen O. Chemical-shift artifact reduction in Hadamard-encoded MR spectroscopic imaging at high (3T and 7T) magnetic fields. *Magn Reson Med* 2007;58(1):167-173.
  26. Li BS, Regal J, Gonen O. SNR versus resolution in 3D 1H MRS of the human brain at high magnetic fields. *Magn Reson Med* 2001;46(6):1049-1053.
  27. Li S, Dardzinski BJ, Collins CM, Yang QX, Smith MB. Three-dimensional mapping of the static magnetic field inside the human head. *Magn Reson Med* 1996;36(5):705-714.
  28. Mareci TH, Brooker HR. Essential considerations for spectral localization using indirect gradient encoding of spatial information. *J Magn Reson* 1991;92(2):229-246.
  29. Brooker HR, Mareci TH, Mao JT. Selective Fourier transform localization. *Magn Reson Med* 1987;5(5):417-433.
  30. Goelman G, Liu S, Gonen O. Reducing voxel bleed in Hadamard-encoded MRI and MRS. *Magn Reson Med* 2006;55(6):1460-1465.
  31. Marion D, Ikura M, Bax A. Improved solvent suppression in one- and two-dimensional NMR spectra by convolution of time domain data. *J Magn Reson* 1989;84(2):425-430.
  32. Gonen O, Murdoch JB, Stoyanova R, Goelman G. 3D multivoxel proton spectroscopy of human brain using a hybrid of 8th-order Hadamard encoding with 2D chemical shift imaging. *Magn Reson Med* 1998;39(1):34-40.
  33. Ashburner J, Friston K. Multimodal image coregistration and partitioning: a unified framework. *Neuroimage* 1997;6(3):209-217.
  34. Ashburner J, Friston KJ. Voxel-based morphometry: the methods. *Neuroimage* 2000;11(6 Pt 1):805-821.
  35. Soher BJ, Young K, Govindaraju V, Maudsley AA. Automated spectral analysis III: application to in vivo proton MR spectroscopy and spectroscopic imaging. *Magn Reson Med* 1998;40(6):822-831.
  36. Inglese M, Li BS, Rusinek H, Babb JS, Grossman RI, Gonen O. Diffusely elevated cerebral choline and creatine in relapsing-remitting multiple sclerosis. *Magn Reson Med* 2003;50(1):190-195.
  37. Träber F, Block W, Lamerichs R, Gieseke J, Schild HH. 1H metabolite relaxation times at 3.0 tesla: measurements of T1 and T2 values in normal brain and determination of regional differences in transverse relaxation. *J Magn Reson Imaging* 2004;19(5):537-545.
  38. Kirov II, Fleysher L, Fleysher R, Patil V, Liu S, Gonen O. Age dependence of regional proton metabolites T2 relaxation times in the human brain at 3 T. *Magn Reson Med* 2008;60(4):790-795.
  39. Posse S, Otazo R, Caprihan A, et al. Proton echo-planar spectroscopic imaging of J-coupled resonances in human brain at 3 and 4 Tesla. *Magn Reson Med* 2007;58(2):236-244.
  40. Todtenkopf MS, Vincent SL, Benes FM. A cross-study meta-analysis and three-dimensional comparison of cell counting in the anterior cingulate cortex of schizophrenic and bipolar brain. *Schizophr Res* 2005;73(1):79-89.
  41. Bouras C, Kövari E, Hof PR, Riederer BM, Giannakopoulos P. Anterior cingulate cortex pathology in schizophrenia and bipolar disorder. *Acta Neuropathol (Berl)* 2001;102(4):373-379.
  42. Cotter D, Mackay D, Landau S, Kerwin R, Everall I. Reduced glial cell density and neuronal size in the anterior cingulate cortex in major depressive disorder. *Arch Gen Psychiatry* 2001;58(6):545-553.
  43. Chana G, Landau S, Beasley C, Everall IP, Cotter D. Two-dimensional assessment of cytoarchitecture in the anterior cingulate cortex in major depressive disorder, bipolar disorder, and schizophrenia: evidence for decreased neuronal somal size and increased neuronal density. *Biol Psychiatry* 2003;53(12):1086-1098.
  44. Kane JM, Correll CU. Past and present progress in the pharmacologic treatment of schizophrenia. *J Clin Psychiatry* 2010;71(9):1115-1124.
  45. Mikkelsen JD, Thomsen MS, Hansen HH, Lichota J. Use of biomarkers in the discovery of novel anti-schizophrenia drugs. *Drug Discov Today* 2010;15(3-4):137-141.
  46. Wood SJ, Yücel M, Wellard RM, et al. Evidence for neuronal dysfunction in the anterior cingulate of patients with schizophrenia: a proton magnetic resonance spectroscopy study at 3 T. *Schizophr Res* 2007;94(1-3):328-331.
  47. Ende G, Braus DF, Walter S, et al. Effects of age, medication, and illness duration on the N-acetyl aspartate signal of the anterior cingulate region in schizophrenia. *Schizophr Res* 2000;41(3):389-395.
  48. Ongür D, Prescott AP, Jensen JE, Cohen BM, Renshaw PF. Creatine abnormalities in schizophrenia and bipolar disorder. *Psychiatry Res* 2009;172(1):44-48.
  49. Tayoshi S, Sumitani S, Taniguchi K, et al. Metabolite changes and gender differences in schizophrenia using 3-Tesla proton magnetic resonance spectroscopy (1H-MRS). *Schizophr Res* 2009;108(1-3):69-77.